ESCUELA DE CONSTRUCCIÓN CIVIL
FACULTAD DE INGENIERÍA
Revista de la Construcción
Journal of Construction

Research Article

Nonlinear finite element analysis of steel fiber reinforced concrete beams subjected to impact loads

Ahmet Hamdi Serdar[1], Naci Caglar*[2,3], Gamze Demirtas[2], Mehmet Saribiyik[1]

1 Sakarya University of Applied Science, Sakarya (Türkiye); aserdar@subu.edu.tr
2 Sakarya University, Sakarya (Türkiye); caglar@sakarya.edu.tr
3 Bursa Technical University, Bursa (Türkiye); caglar@btu.edu.tr
4 Sakarya University, Sakarya (Türkiye); demirtas@sakarya.edu.tr
5 Sakarya University of Applied Science, Sakarya (Türkiye); mehmets@subu.edu.tr
*Corresponding author: caglar@sakarya.edu.tr (N. Caglar)

Received: 11.04.2023; **Accepted:** 17.12.2023; **Published:** 25.04.2024

Citation: Serdar, A., Caglar, N., Demirtas, G., Saribiyik, M. (2024). Nonlinear finite element analysis of steel fiber reinforced con-crete beams subjected to impact loads. Revista de la Construcción. Journal of Construction, 23(1), 88-103. https://doi.org/10.7764/RDLC.23.1.88

Abstract: Steel fiber reinforced concrete, compared to the conventional concrete; is a composite building material that performs much better in terms of parameters such as ductility, energy absorption capacity, fracture toughness, fatigue resistance, and the use of steel fiber reinforced concrete (SFRC) in structures has become widespread. In this study, a nonlinear finite element model (FEM) has been developed that can represent the behavior of beams produced by using steel fiber concrete subjected to impact load. For this purpose, a finite element model of beam series produced with fiber-reinforced concrete obtained from the literature was created. The ABAQUS package program was used to create models simulating the behavior. Numerical results showed that the model could successfully capture the experimental results of beams selected from the literature. In addition to simulation, a parametric study was also performed to investigate the effect of stirrups, reinforcement ratio, and drop height on the behavior of SFRC beams under impact loads. The results of the parametric study showed that increasing the fiber ratio and reinforcement ratio positively affected the behavior of SFRC beams in terms of displacement recovery.

Keywords: steel fiber reinforced concrete, RC beam, impact load, nonlinear finite element analysis.

1. Introduction

The conventional concrete has a relatively weak energy absorption capacity due to its brittle form, its behavior against sudden loading remains weak. In many studies, to improve the energy absorption capacity of conventional concrete, the method of incorporating steel wire into the concrete matrix has been applied. However, these studies have generally studied the static behavior (Grime, 1934; Ezeldin and Balaguru, 1992; Casanova and Rossi, 1997; Yılmaz et al., 2023; Chen and May, 2009; Kantar et al., 2011; Tokgöz et al.,2015; Ulzurrun and Zanuy, 2017; Yoo et al, 2017; Najah, 2018; Monteiro et al., 2018; Demirtaş, 2019; Naraganti et al., 2019; Dok et al., 2020; Li et al., 2021; Sivakumar et al., 2020; Saravanakumar et al., 2021; Dok et al., 2021; Shaaban et al., 2021; Meng et al., 2021; Melo et al., 2021)

Steel fiber concrete, compared to the conventional concrete; is a composite building material that performs much better in terms of parameters such as ductility, energy absorption capacity, fracture toughness, and fatigue resistance. Its characteristic tensile strength is greater than the conventional concrete. It is known that the high ductility and tensile strength of steel fiber reinforced concrete (SFRC) are due to the bridging effect of the fibers across cracks (Ezeldin and Balaguru, 1992). Due to these properties, steel fiber concrete is considered as a suitable material for critical structures, military facilities, transportation infrastructure, and reinforced concrete structures exposed to dynamic loads (Casanova and Rossi, 1997).

Steel fiber reinforced concrete (SFRC) is obtainment in structural engineering due to its enhanced impact resistance, ductility, and energy absorption capabilities. In recent experiments, twelve SFRC beams were subjected to impact loading at their midpoints. Varying stirrup ratios and steel fiber content provided a comprehensive study of their dynamic and mechanical behavior. Investigations in conjunction with impact force and mid-span displacement records demonstrated significant improvements in the impact resistance of SFRC beams, including improved crack patterns, ductility and energy absorption. Finite element analyses and experimental results showed significant agreement, thus providing additional validation to the findings (Vivas et al, 2022). In addition, a study on fiber-reinforced concrete (FRC) proposed a new test method to evaluate the material behavior of the initial crack and post-crack phases. Analysis of the effects of compressive strength of FRC on impact behavior indicated the importance of fiber properties in impact resistance. Research in this field advances the assessment of impact resistant materials and provides information on their mechanical behavior under dynamic loading conditions (Jin et al, 2018).

Many studies have been carried out to determine the behavior of structural system elements produced with SFRC under the influence of static loads (Tokgöz, 2015). Ezeldin and Balaguru (1992) produced reinforced concrete beam series using SFRC to determine the stress-strain behavior. Within the scope of the study, parameters such as maximum stress, modulus of elasticity, concrete toughness, and stress-strain behavior of the series were examined. They observed that the steel fiber in the fibrous concrete increased the toughness and energy absorption capacity of the concrete. Casanova and Rossi (1997) studied steel fiber additives' shear strength and crack propagation in normal strength and high strength concretes. They demonstrated that the fiber additive was more beneficial than stirrups against cracks that may occur in the joints of the carrier system elements and provided greater moment carrying capacity. They noticed that fibrous concretes provided significant improvements in strength, ductility, and energy consumption compared to the conventional concrete. Tokgöz (2015), in their study, added steel fibers to the concrete in an attempt to investigate the effects on the ductility, deformation, and winding properties of the columns. It was concluded that the shear strength of the SFRC beams depended highly on the tensile stress of the fiber concrete, therefore the geometry of the structural element directly affected its characteristic properties.

Earlier studies on the impact loading revealed that the strength of the concrete material changed depending on the loading speed (Grime, 1934). In the following years, a new type of concrete obtained by adding different materials to the concrete matrix was investigated under the impact (Ulzurrun and Zanuy, 2017). Altun et al. (2006) produced and tested standard cylinder pressure specimens and beam bending specimens to determine the static and dynamic behavior of SFRC. As a result of the experiments, it was stated that the fiber-reinforced concrete exhibited more ductile behavior, reduced the risk of cracking, and performed better depending on the fiber ratio against the bursting effect compared to the conventional concrete. Chen and May (2009) investigated the behavior of beam and floor elements under high mass and low-velocity impact. They observed local damages in the form of scattering and shedding in the beam and slab series, and as a result of the experiments, they determined the values of impact load, acceleration, and reinforcement unit strain. Saatci and Vecchico (2009) performed impact tests by free-dropping 2 different masses at the midpoint of 8 reinforced concrete beams with different shear reinforcements. In the study examining the cutting behavior, they noticed that the damage occurred in the form of a shear cone.

The main purpose of this study is to investigate the behavior of SFRC beams under the impact loads. ABAQUS was used to generate nonlinear finite element models (FEM). Experimental studies selected from the literature were used to validate the finite element model of SFRC beams. In the finite element models confirmed by the experimental study results, a parametric study was carried out by selecting the longitudinal reinforcement ratio, fiber ratio, volumetric stirrup ratio, and impact height data as variables.

2. Experimental study

An experimental study selected from the literature was used to validate the nonlinear finite element model (Ulzurrun and Zanuy, 2017). In the experimental study carried out by Ulzurrun and Zanuy (2017), the beam specimens had a rectangular section of 125x250 mm with a span of 2 m. Two ribbed longitudinal reinforcements with a diameter of 16 mm were placed in the compression and tension zone. There were no stirrups in the beams, the shearing effect was compensated by the steel fibers in the concrete matrix and its schematic representation is given in Figure 1. The material properties of the B and E series, for which finite element models were created, are given in Table 1. In the experimental study, the B and E series had a steel fiber ratio of 0.50% and 1.00%, respectively. In the experimental study, dynamic tests were carried out on the series by the impact load applied to the beam by the free fall of the 200 kg striking head from a height of 1.75 m.

Table 1. Concrete material properties (Ulzurrun and Zanuy, 2017).

	Fiber ratio (%)	Fiber type	Fiber length/ fiber diameter (mm)	Fiber yield strength (MPa)	Compressive strength (MPa)	Indirect tensile strength (MPa)	Fracture energy (kN/m)
B	0.50	Hooked	60/1.00	830	59.4	6.1	3.14
E	1.00	Hooked	60/1.00	830	52.1	7.0	6.65

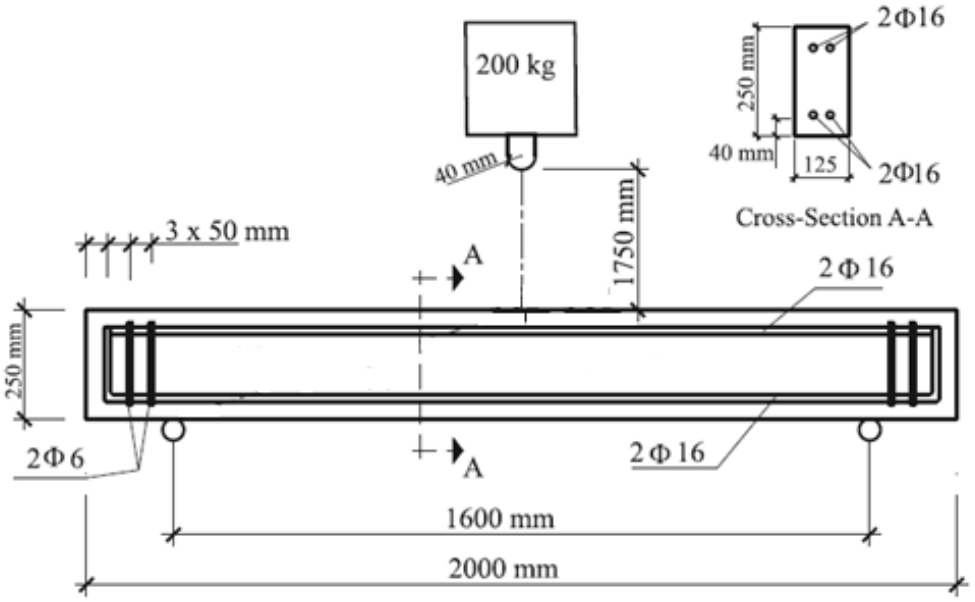

Figure 1. Beam geometry and cross-section (Ulzurrun and Zanuy, 2017).

3. Nonlinear finite element model

The finite element model of the experimental study carried out by Ulzurrun and Zanuy (2017) was created and the results obtained from the experimental study and numerical analyses were compared. In this context, 3D numerical models were created with the ABAQUS finite element program.

3.1. Modeling of concrete

The Concrete damage plasticity (CDP) model was used to describe the nonlinear behavior of the concrete material. The CDP model was first introduced by Lubliner for monotonic loading (Lubliner et al., 1989). It was later modified by Fenves for cyclic and dynamic loadings (Lee et al., 1998). In the CDP Model, two failure mechanisms are defined, namely crushing of concrete and tensile fracture. The most important parameters required to create a CDP model to accurately represent the

material behavior are the uniaxial stress-strain curves under compression and tension. The details of the parameter are discussed as follows.

3.1.1. Yield function

The elastic limits under possible stress combinations in concrete are determined by a yield surface. The yield surface envelope under plane stress used in the CDP model is given in Figure 2.

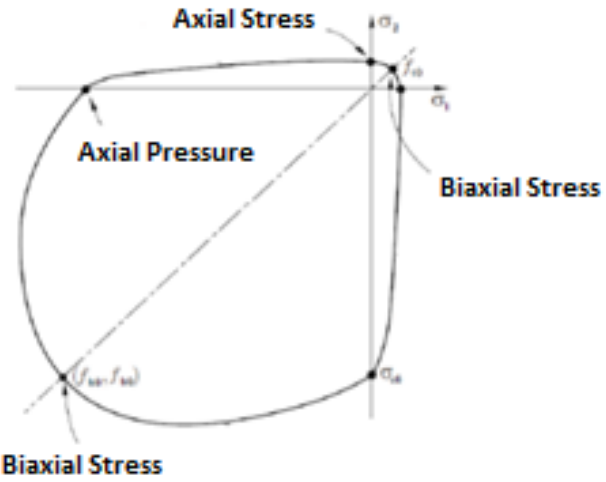

Figure 2. Biaxial stress-strain envelope of concrete (Sümer, 2010).

Parameters to form the yield surface of concrete are the ratio of the biaxial initial compressive yield stress to the uniaxial initial compressive stress *(σ_{bo}/σ_{co})*, the eccentricity parameter *(∈)*, the dilation angle *(ψ)*, and the secondary constant stress ratio on the tensile function *(Kc)*. The default value for the eccentricity parameter *(∈)* is given as 0.1 in the program. The σ_{bo}/σ_{co}ratio takes values between 1.10 and 1.16 (Lubliner et al., 1989). The default value for the Kc value is given as 2/3. The dilation angle *(ψ)* represents the plastic volumetric change.

3.1.2. Viscoplastic regulation

Material models that exhibit stress and stiffness reduction often create convergence problems in analysis. To overcome this convergence problem, viscoplastic arrangement was made. With the definition of viscoplasticity, convergence was achieved by allowing the stresses to go slightly outside the yield surface. The default value of the viscosity parameter is given as 0 in the ABAQUS program. A value of 0 means no viscoplastic regulation (Hibbitt, 2013).

3.1.3. Plastic flow

The yield potential, G, which defines the relationship between the plastic strain increase and the stress increase in the CDP model, is defined by the Drucker-Prager hyperbolic function (Figure 3).

$$G = \sqrt{(\in.\sigma_{t0}tan\psi)^2 + \bar{q}^2} - \bar{p}.tan\psi \quad (1)$$

where; ∈: Yield surface eccentricity, ψ: dilation angle measured in the $p-q$ plane, $\bar{q}$: Equivalent mises effective stress, σto: Maximum tensile stress, $\bar{p}$: Expresses the hydrostatic compressive stress (Sümer, 2010).

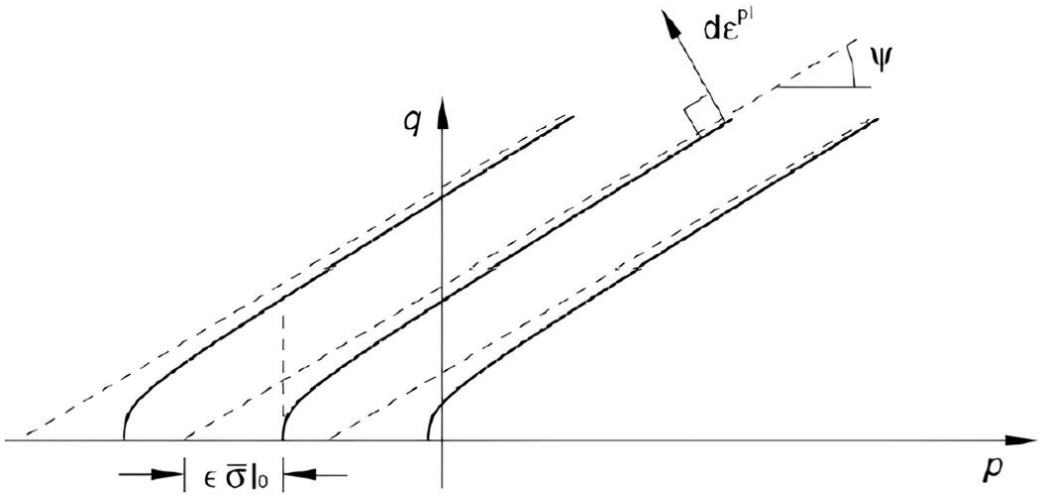

Figure 3. Drucker-Prager hyperbolic function (Sümer, 2010; Hibbitt, 2013).

The relationship between compressive stress and strain of concrete, inelastic and plastic strain is defined as shown in Fig. 4.a. Under uniaxial compressive loading, the CDP model exhibits a linear behavior up to σ_{c0} (Figure 4). When this strength is exceeded, plastic deformations begin in the concrete. The behavior between σ_{c0} and σ_{cu} is expressed as strength hardening, and the behavior after exceeding σcu is expressed as strength softening (Hibbitt, 2013). As seen in Figure 4.a, the behavior of the CDP model under uniaxial tension is defined by the linear elastic stress-strain relationship until the concrete reaches the maximum tensile stress (σ_{t0}). Tensile cracking occurs in concrete when the stress reaches this value. The part where the strength starts to decrease with the propagation of cracks is defined as the tensile stiffness and can be expressed with a decreasing stress-strain relationship or fracture energy (Earij et al., 2017).

In Figure 4, E_0 presents the initial modulus of elasticity, $\tilde{\varepsilon}_c^{pl}$ is the compression plastic strain, $\tilde{\varepsilon}_t^{pl}$corresponds to the tensile plastic strain, ε_c^{in} implies the compression inelastic strain, and εt-ck denotes the cracking unit strain. The relationship between the stress and strain is expressed in Equations 2 and 3 in terms of these parameters.

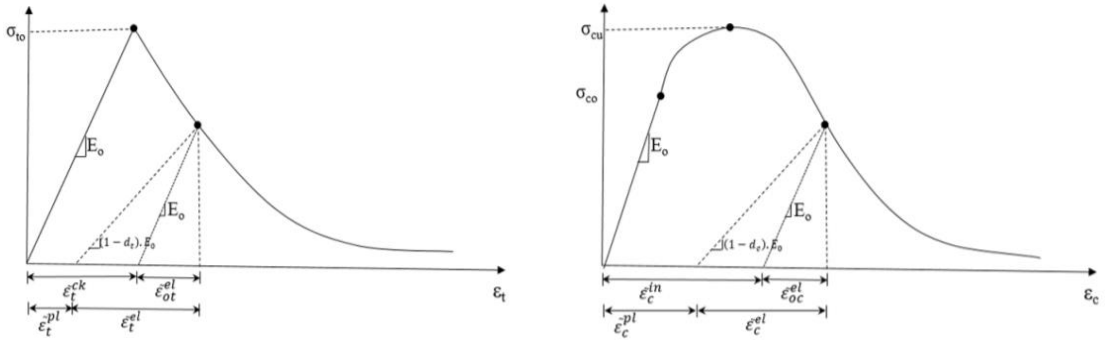

(a) (b)

Figure 4. The behavior of concrete under axial tension (a), and compression (b) (Hibbitt, 2013).

$$\sigma_c = (1 - d_c).E_0.(\varepsilon_c - \tilde{\varepsilon}_c^{pl}) \quad (2)$$

$$\sigma_t = (1 - d_t).E_0.(\varepsilon_t - \tilde{\varepsilon}_t^{pl}) \quad (3)$$

The fracture surface is controlled by two variables $(\tilde{\varepsilon}_t^{pl} - \tilde{\varepsilon}_c^{pl})$ that depend on the fracture mechanism under compressive and tensile loadings. Concrete stress-strain behavior can be obtained from experimental studies or model stated in the literature

(Mander et al., 1984; SETRA AFGC, 2002; CEB-FIB, 2010). The stress-strain $(\sigma - \varepsilon)$ values must be introduced to the program as stress-inelastic strain $(\sigma - \varepsilon_c^{in})$. Defined values are automatically converted to stress-plastic strain $(\sigma - \tilde{\varepsilon}_c^{pl})$ values by the program. These values are defined by Equation 4 -7.

$$\varepsilon_c^{in} = \varepsilon_c - \frac{\sigma_c}{E_0} \tag{4}$$

$$\tilde{\varepsilon}_c^{pl} = \tilde{\varepsilon}_c^{in} - \frac{d_c}{(1-d_c)} \cdot \frac{\sigma_c}{E_0} \tag{5}$$

$$\varepsilon_t^{ck} = \varepsilon_t - \frac{\sigma_t}{E_0} \tag{6}$$

$$\tilde{\varepsilon}_t^{pl} = \tilde{\varepsilon}_t^{ck} - \frac{d_t}{(1-d_t)} \cdot \frac{\sigma_t}{E_0} \tag{7}$$

d_c and d_t are damage parameters expressing the decrease in elastic stiffness of concrete under the effect of compressive and tensile stresses and are expressed by Equations 8 and 9 (Birtel and Mark, 2006). The damage parameter value changes between 0 and 1, where 0 means no damage and 1 implies fully damaged.

$$d_c = 1 - \frac{\sigma_c/E_0}{\sigma_c/E_0 + \varepsilon_c^{in}(1-b_c)} \tag{8}$$

$$d_t = 1 - \frac{\sigma_{t0}/E_0}{\sigma_{t0}/E_0 + \varepsilon_c^{ck}(1-b_t)} \tag{9}$$

3.2. Reinforcement model

The "classical metal plasticity" model, one of the material models included in the program, was used to define the mechanical behavior of the steel reinforcement. For the classical metal plasticity model, the behavior should be defined as stress-plastic strain. For this reason, it is necessary to obtain a stress-plastic strain graph by subtracting the elastic strain from the total strain value. Mander et al. (1984) in the literature to describe the stress-strain curve of reinforcement (Figure 5).

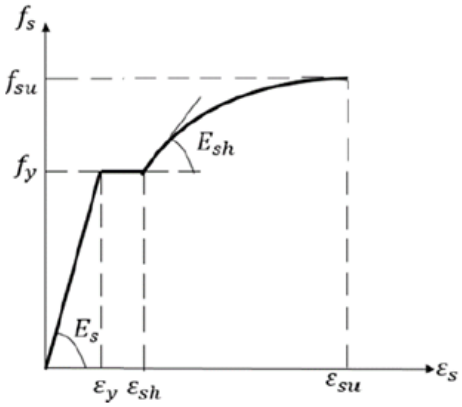

Figure 5. Reinforcement stress-strain diagram (Mander et al., 1984).

The necessary equations to describe the behavior are explained below.

Elastic loading *(0 ≤ εs ≤ εy)*

$$f_s = E_s . \varepsilon_s \tag{10}$$

Yield region *(ε_y<ε_s≤ε_{sh})*

$$f_s = f_y \tag{11}$$

Strength hardening *(ε_{sh}<ε_s<ε_{su})*

$$f_s = f_{su} + (f_y - f_{su}) \left| \frac{\varepsilon_{su} - \varepsilon_s}{\varepsilon_{su} - \varepsilon_{sh}} \right|^p \tag{12}$$

Where; f_s: Stress in reinforcing steel, ε_s: Reinforcement unit deformation, E_s: Rebar modulus of elasticity, ε_y: Yield strain of reinforcing steel, fy: Yield strength of reinforcement, f_{su}: Reinforcement ultimate strength, ε_{su}: Rebar rupture strain, ε_{sh}: Reinforcement strain at the onset of strength hardening, p: Strength hardening strength.

3.2.1. Reinforcement concrete interaction

The interaction between reinforcement and concrete was provided by the embedded element technique. According to this technique, the rotation degrees of freedom of the nodes of the embedded element is limited by the degrees of freedom of the host element.

3.3. Geometry and boundary conditions of finite element models

In the solid model created, concrete is modeled as linear finite elements with 8-node points and reduced integration (C3D8R). The reinforcement bars are modeled as 3-dimensional linear finite element segments with 2-node points (T3D2). In the RC beam design, the supports at both ends are defined as linear.

The vertical movement of the right support and the vertical and horizontal movement of the left support are prevented. Mesh structure of the model was determined by sensitivity analysis and 50 mm was chosen.

3.4. Loading conditions

The impact loading was created by the drop weight of 200 kg, which was modeled as a rigid body and defined by reference from the midpoint of the body whose mass was modeled. The drop weight moves on the RC beam in the vertical direction with the effect of gravity.

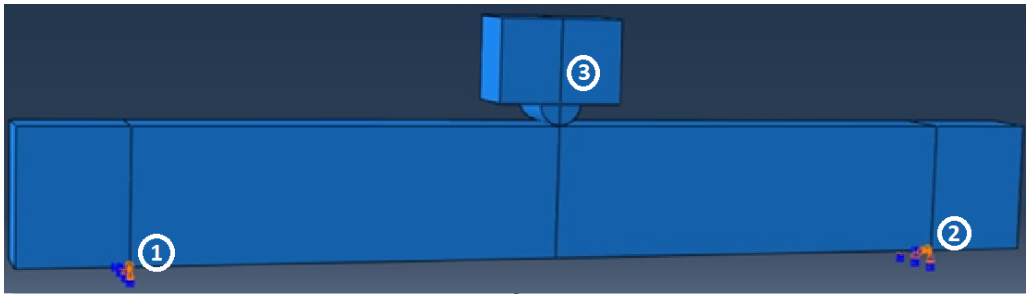

Figure 6. The geometry of dynamic model (1. fixed support, 2. roller support, 3. drop weight) (Serdar et al., 2021).

4. Validation of the finite element model

Results of the nonlinear finite element model and the experimental results performed by Ulzurrun and Zanuy (2017) are presented in Figure 7 and Figure 8. Impact load-Time and Displacement-Time are given in the figures.

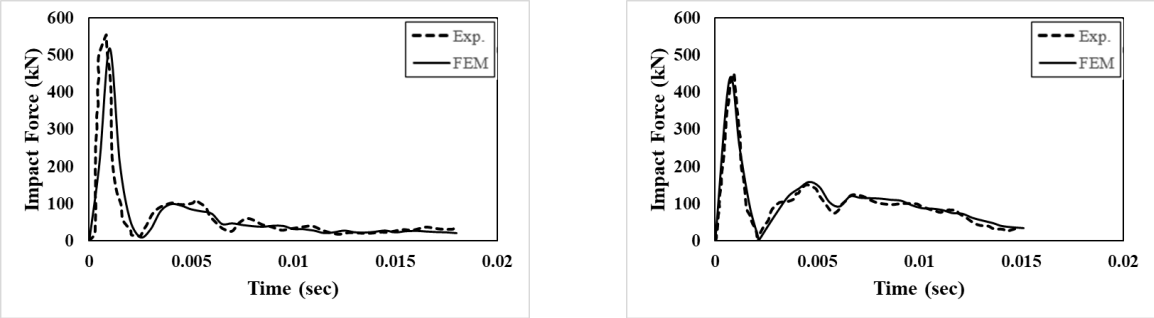

(a) B Series (b) E Series

Figure 7. Impact load-time of: (a) B, and (b) E series.

In order to understand that FEM gives accurate results, FEM results and experimental results should be compared. If the difference between the experimental and FEM results is 10% or less, the FEM is considered to be accurate. Impact loading-time graphs of B and E series are given in Figure 7(a) and Figure 7 (b). It is clear that FEM provides model simulation without any problem, showing very similar results in damping of dynamic motion both in terms of value and duration (Badshah and Badshah, 2020; Wu et al., 2022). Impact loading-time graphs of B and E series are given in Figure 7 (a) and Figure 7 (b) It is clear that FEM provides model simulation without any problem, showing very similar results in damping of dynamic motion both in terms of value and duration.

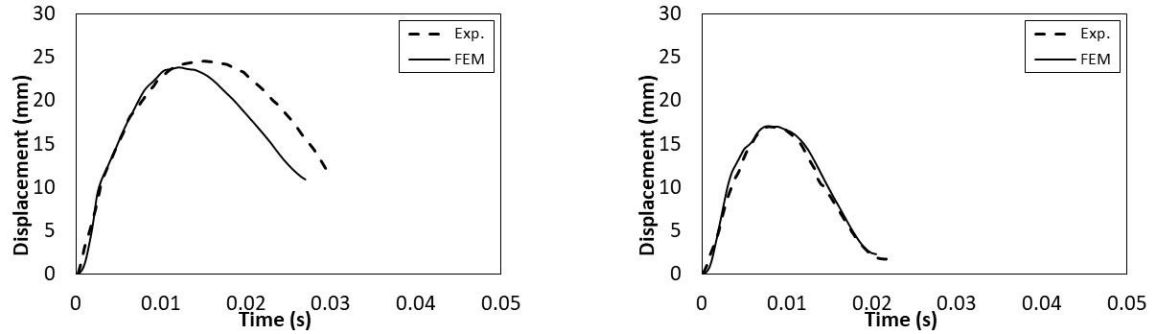

(a) B Series (b) E Series

Figure 8. Impact load-time of: (a) B, and (b) E Series.

The displacement-time graphs of B and E series are given in Figure 8 (a) and Figure 8 (b). It is seen that the experimental and numerical analysis results of the E series, which has 1.0% steel wire in its matrix, are largely the same (Figure 9 (b)). When the results of B series, which has 0.5% steel wire in its matrix, are examined, a slight difference is observed between experimental and numerical analysis in terms of dynamic time. However, since this difference is around 0.003 sec and is negligible, it is seen that there is a very high level of similarity in the results (Figure 9 (a)). Therefore, as can be seen from these results, the nonlinear finite element model is quite successful in simulating the real behavior of reinforced concrete beams produced with steel fiber concrete under impact loads.

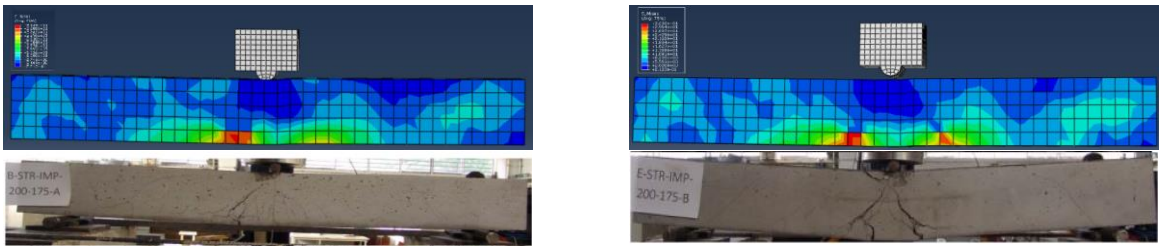

(a) B Series (b) E Series

Figure 9. Crack Growth (top: FEM, bottom: experiment) (Ulzurrun and Zanuy, 2017).

Table 2. Comparison of test and FEM results.

	Kinetic Energy (kJ)		Velocity (m/s)		Impact load (kN)		Maximum displacement (mm)	
	Exp.	FEM	Exp.	FEM	Exp.	FEM	Exp.	FEM
B Series	3.43	3.46	5.86	5.86	565	469	23.84	24.48
E Series	3.43	3.45	5.86	5.86	497	561	17.03	17.05

The crack distribution formed as a result of the analysis and the crack distribution formed in the beam series as a result of the experimental study are given in Figure 9 for B and E series. Experimentally and numerically formed cracks occur at the midpoint of the beam.

5. Parametric study

A parametric study was carried out to determine the behavior of the reinforced concrete beam produced with steel fiber concrete against the impact loading. In this study, series with different transverse and longitudinal reinforcement ratios and different loading rates were examined. As tensile reinforcement, 2ϕ12, 2ϕ16, 2ϕ20 diameter longitudinal reinforcement bars were selected. The diameter of the stirrup reinforcement was selected as ϕ8, the reinforcement configuration was modelled with 3 different stirrups. This study modelled with non-stirrups, stirrups at 100 mm and stirrups at 200 mm, respectively.

The midpoint displacement and crack distribution of the generated models were used as data for the evaluation of the behavior. Within the scope of the parametric study, material properties, beam cross-section, free span, support conditions were kept constant; transverse and longitudinal reinforcement ratios and drop height were chosen as the working variables (Table 3).

Table 3. The selected variables for parametric study

	Fiber ratio (%)	Rebar Dia.	Drop height (m)	Stirrups mm
B Series	0.50	2ϕ12	1.00	Non-stirrup / 200 / 100
			1.75	Non-stirrup / 200 / 100
			2.50	Non-stirrup / 200 / 100
		2ϕ16	1.00	Non-stirrup / 200 / 100
			1.75	Non-stirrup / 200 / 100
			2.50	Non-stirrup / 200 / 100
		2ϕ20	1.00	Non-stirrup / 200 / 100
			1.75	Non-stirrup / 200 / 100
			2.50	Non-stirrup / 200 / 100
E Series	0.50	2ϕ12	1.00	Non-stirrup / 200 / 100
			1.75	Non-stirrup / 200 / 100
			2.50	Non-stirrup / 200 / 100
		2ϕ16	1.00	Non-stirrup / 200 / 100
			1.75	Non-stirrup / 200 / 100
			2.50	Non-stirrup / 200 / 100
		2ϕ20	1.00	Non-stirrup / 200 / 100
			1.75	Non-stirrup / 200 / 100
			2.50	Non-stirrup / 200 / 100

The outputs of the nonlinear analysis performed on B and E series with 0.5% and 1% fiber ratios are shown in mid-point displacement (Figures 10, 11, and 12) for three different tensile reinforcement ratios and three different drop heights.

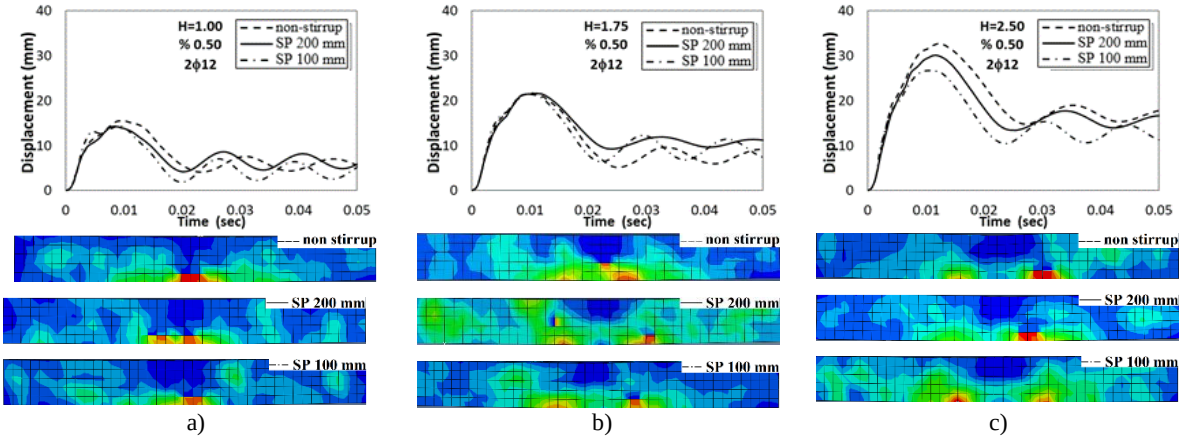

Figure 10. The behavior of B Series beam models with fixed longitudinal reinforcement and fixed drop heights and different stirrup pitch.

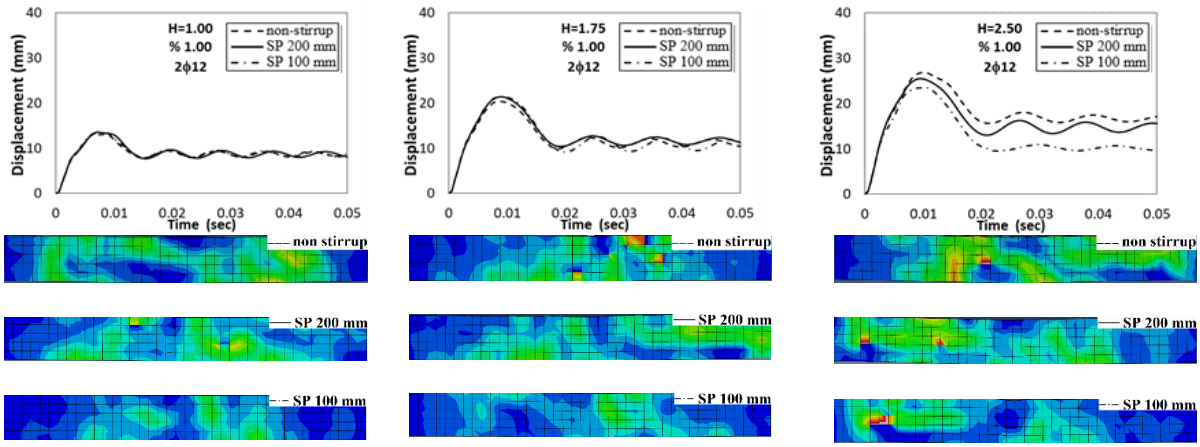

a) b) c)

Figure 11. The behavior of E Series beam models with fixed longitudinal reinforcement and fixed drop heights and different stirrup pitch.

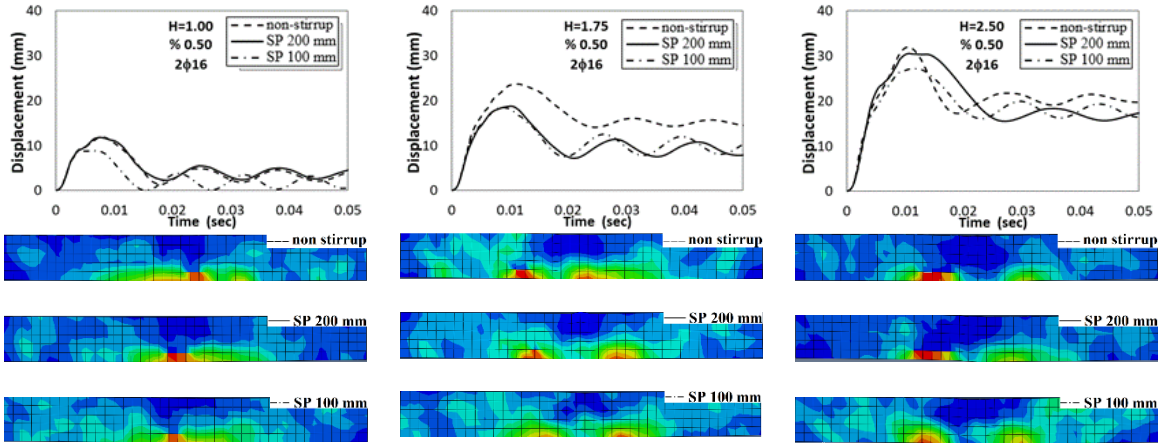

a) b) c)

Figure 12. The behavior of B Series beam models with fixed longitudinal reinforcement and fixed drop heights and different stirrup pitch.

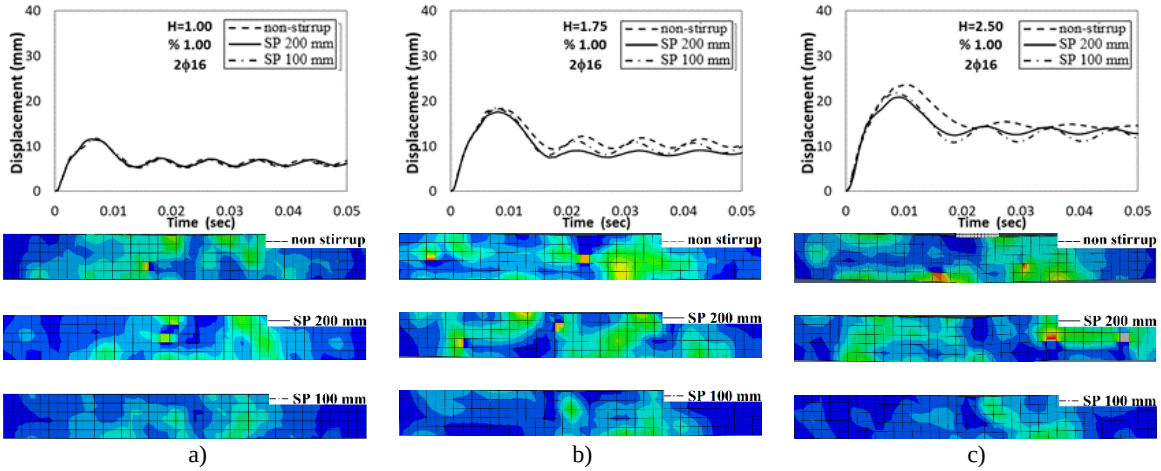

Figure 13. The behavior of E Series beam models with fixed longitudinal reinforcement and fixed drop heights and different stirrup pitch.

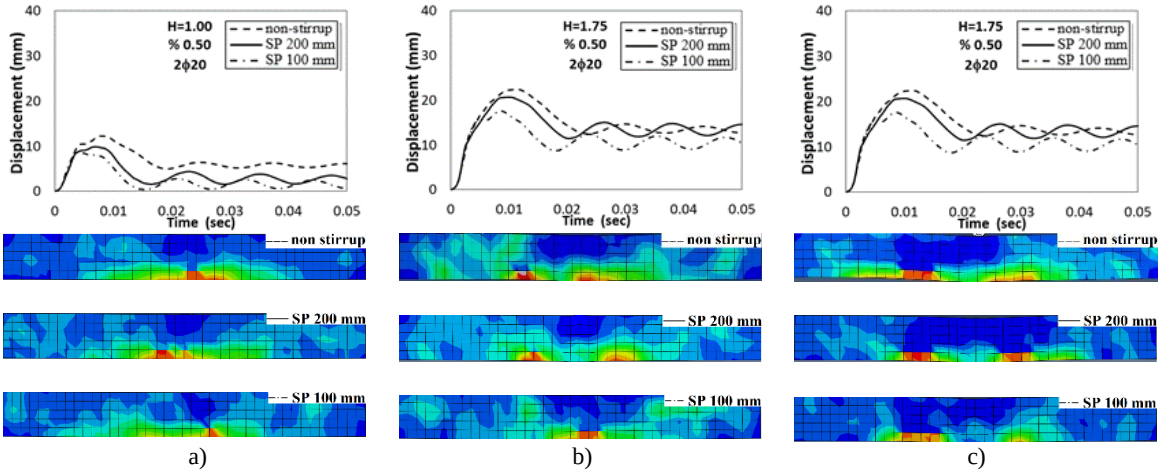

Figure 14. The behavior of B Series beam models with fixed longitudinal reinforcement and fixed drop heights and different stirrup pitch.

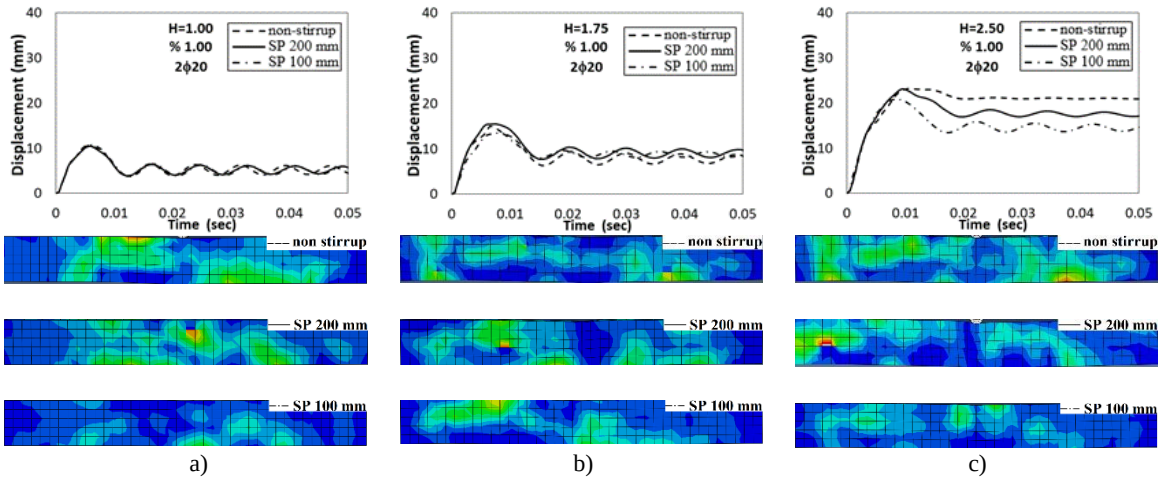

Figure 15. The behavior of E Series beam models with fixed longitudinal reinforcement and fixed drop heights and different stirrup pitch.

When Figures 10-15 is examined carefully, it is realized that the increase in fiber and reinforcement ratios positively affect the behavior in terms of the displacement recovery. The displacement recovery indicates the elastoplastic behavior resulting from the increase in the difference between the maximum displacement and the ultimate displacement. As can be seen especially from the series subjected to high impact energy, displacement recovery was observed significantly with the increase in the fiber ratio in the concrete matrix. As the tensile reinforcement ratio increased in reinforced concrete beams, vertical displacements decreased up to 40%. In the series where the fiber ratio was 0.5% (B series), an increase in damage formation occurred when the drop height increased from 1m to 2.5m.

An increase of approximately 120% occurred in the maximum vertical displacements. In the series with a fiber ratio of 1.0% (E series), these increases were limited to 80%. In other words, the displacements decreased with increasing fiber ratio. In the series with a fiber ratio of 0.50%, local damage is observed as the drop height increases. In the series with a fiber ratio of 1.00%, it is seen that the impact on the beam is transferred to the beam as a result of the bridging effect of the fibers and local damage formation is limited. The fibers act as a bridge over which stresses pass. In accordance with the work of Baradan (2012) and Saravanakumar (2021), with the increase of the fiber content in the concrete matrix, the bridging effect of the fibers becomes more pronounced (Figures 10-15). As a result of this effect, the cracks remain at the capillary level, preventing stress concentration and spreading the resulting stresses across the beam.

As the drop height increased, residual and maximum displacements increased. In the series subjected to high drop height, more displacement occurred depending on the tensile reinforcement ratio. However, the results obtained from the series with high fiber ratio (Specimen E) showed that reductions in maximum and residual deformations occurred even at high drop heights. In the series modelled with the same reinforcement configuration, it was determined that the effect of the stirrups decreased in case of high fiber ratio and the stresses generated were absorbed by the fibers.

It is understood that the need for stirrups is limited at low heights, but the specimens are stressed more as the drop height increases. Therefore, as the drop height increases, the behavior of the series is seen more clearly and distinctly.

The drop height, which is selected as one of the variable parameters in determining the behavior, has a very important position in the interpretation of the results obtained.

Differences are observed in the vertical displacements of the series produced non-stirrups, with 200 mm stirrups and 100 mm stirrups. In the series produced with 0.5% fiber and 200 mm spacing, vertical displacements decreased between 15% and 25% compared to the series no stirrups. In the series with 100 mm spacing, the reductions in vertical displacements reached between 30% and 50% compared to the specimens no stirrups. In the series produced with 1.00% fiber and 200 mm spacing, vertical displacement values decreased between 8% and 20% compared to the series without stirrups. In the series with 100

mm spacing, the reductions in vertical displacement values reached values between 15% and 25% compared to the specimens without stirrups. As a result, the reduction in vertical displacements reaches 50% in the series with 0.5% fibers and 25% in the series with 1.0% fibers. Therefore, the contribution of the stirrup to the vertical displacement of the reinforced concrete beam is more pronounced in the 0.5% fiber series. It is known that the loads on the beam are also resisted by the fibers (Shaaban at al., 2021). Therefore, the rate of decrease of the vertical displacement with the increase of the stirrup in the 1.0% fiber series is less than that of the 0.5% fiber series. However, the maximum vertical displacements in the 1.0% fiber series with no stirrups are similar to the 0.5% fiber series with stirrups. In the 0.50% fiber series, the vertical displacements decreased by about 40% with the increase of tensile reinforcement. This decrease was obtained for all types of stirrups. As the drop height increased, the vertical displacements increased approximately 2.5 times. In the series with increased tensile reinforcement ratio, the vertical displacements increased about 2 times with the increase in drop height. In the series with 1.00% fiber ratio, the vertical displacements decreased about 20% with the increase in tensile reinforcement. As the drop height increased, the vertical displacements increased nearly 2 times. In the series with a high ratio of tensile reinforcement, the change in vertical displacements with the increase of the drop height is about 40%.

As a result, it is understood that the contribution of the stirrup in the reinforced concrete system can be compensated by increasing the content of fiber in the concrete matrix. Since the fibers in the concrete matrix limit the expansion of cracks in the concrete with the bridging effect, they meet the stresses caused by the impact load together with the tensile reinforcement and significantly affect the beam behavior positively.

6. Conclusions

In this paper, a nonlinear numerical model was created to simulate the behavior of the SFRC beams subjected to impact loads by using ABAQUS. The nonlinear numerical model was verified with experimental results of selected beams from the literature. The numerical results are observed to be consistent with the experimental results to simulate the nonlinear response of the SFRC beams under impact loads. A parametric study was also performed to investigate the effect of stirrups, reinforcement ratio, and drop height on the response of SFRC beams under impact loads in terms of midpoint displacement versus time. At the end of the parametric study, the following conclusions were derived:

1. Results indicate that increasing the fiber and reinforcement ratios positively influenced the behavior of the beams in terms of displacement recovery. Particularly, the displacement recovery, indicative of elastoplastic behavior resulting from the difference between maximum and ultimate displacements, especially in series subjected to high impact energy. The increase in fiber ratio and tensile reinforcement ratio results in up to 40% reduction in vertical displacement.
2. It was observed that increasing the fiber ratio in the concrete matrix led to a more pronounced bridging effect of the fibers, limiting damage formation and enhancing the beam's capacity to impact loads. The results also revealed that while an increase in drop height resulted in higher residual and maximum displacements, the presence of a high fiber ratio absorption these effects, leading to reductions in deformations even at high drop heights. Increasing the drop height normally increases the level of damage. Here, the amount of fiber ratio also affected the behavior and at 1% fiber ratio, displacement values decreased and damage was reduced.
3. The bridging effect created by the fibers in the concrete matrix becomes more pronounced with the increase of the fiber ratio. Due to this effect, the cracks remain at the capillary level, preventing stress concentration and spreading the resulting stresses across the beam.
4. The vertical displacement reduction reaches 50% for 0.50% fiber series. This value is 25% for 1.00% fiber series. The loads taken by the stirrups are reduced because the cracks in the concrete are limited by the bridging effect of the fibers, and the contribution of the stirrups to the behavior remains at a limited level (Shaaban et al., 2021).
5. Vertical displacements decreased with increasing tensile reinforcement. Tensile stresses are also absorbed by the fibers in the concrete matrix. In the series with 1.0% fibers, the energy absorbed by the fibers is higher. In the series with 1.0% fibers, not all of the stress acts on the tensile reinforcement. Therefore, the decrease in vertical displacements with increasing tensile reinforcement is more obvious in 0.5% fiber specimens.

Nomenclature of Paper

$\in$	Eccentricity parameter	f_s	Stress in reinforcing steel
ψ	Dilation angle	ε_s	Reinforcement unit deformation
Kc	Secondary constant stress ratio on the tensile function	E_s	Rebar modulus of elasticity
G	Yield potential	ε_y	Yield strain of reinforcing steel
$\bar{q}$	Equivalent mises effective stress	fy	Yield strength of reinforcement
E_0	initial modulus of elasticity	f_{su}	Reinforcement ultimate strength
ε_c^{pl}	Compression plastic strain	ε_{su}	Rebar rupture strain
ε_t^{pl}	Corresponds to the tensile plastic strain	ε_{sh}	Reinforcement strain at the onset of strength hardening
ε_c^{in}	Implies the compression inelastic strain	p	Strength hardening strength

References

ABAQUS Research Edition. (2018). Abaqus Unified FEA. Dassault Systèmes SE: 10 rue Marcel Dassault CS 40501 78946 Vélizy-Villacoublay Cedex, France.

Altun F, Yılmaz C, Durmuş A, Kamuran A R I. Investigation of reinforced concrete and steel-fiber reinforced concrete beams under simple bending subjected to blast loading. Erciyes University Journal of the Institute of Science and Technology, 2006, 22(1), 112-120.

Baradan, B., Yazıcı, H., Aydın, S. (2012). Beton. Dokuz Eylül Üniversitesi Mühendislik Fakültesi Yayınları, İzmir, Türkiye.

Birtel, V. A. M. P., & Mark, P. (2006, May). Parameterized finite element modelling of RC beam shear failure. In ABAQUS users' conference (Vol. 14).

Casanova, P., & Rossi, P. (1997). Analysis and design of steel fiber reinforced concrete beams. Structural Journal, 94(5), 595-602.

Chen, Y., & May, I. M. (2009). Reinforced concrete members under drop-weight impacts. Proceedings of the Institution of Civil Engineers-Structures and Buildings, 162(1), 45-56.

de Alencar Monteiro, V. M., Lima, L. R., & de Andrade Silva, F. (2018). On the mechanical behavior of polypropylene, steel and hybrid fiber reinforced self-consolidating concrete. Construction and Building Materials, 188, 280-291.

de Melo, F. M. C., de Jesus Cruz, A. C. A., de Souza Netto, L. D., & de Souza Simplício, M. A. (2021). Experimental study of bond between steel bars and hybrid fibers reinforced concrete. Construction and Building Materials, 275, 122176.

Demirtas, G., Caglar, N., & Sumer, Y. (2022). Nonlinear finite element analysis of ultra-high performance fiber reinforced concrete beams subjected to impact loads.

Dok, G., Caglar, N., Ilki, A., & Yilmaz, C. (2020, October). Effect of impact loading on residual flexural capacity of high-strength reinforced concrete beams. In Structures (Vol. 27, pp. 2466-2480). Elsevier.

Dok, G., Caglar, N., Ilki, A., & Yilmaz, C. (2021). Residual load bearing capacity and failure mechanism of impacted high-strength reinforced concrete shear beams. Engineering Failure Analysis, 121, 105185.

Earij, A., Alfano, G., Cashell, K., & Zhou, X. (2017). Nonlinear three–dimensional finite–element modelling of reinforced–concrete beams: Computational challenges and experimental validation. Engineering Failure Analysis, 82, 92-115.

Ezeldin, A. S., & Balaguru, P. N. (1992). Normal-and high-strength fiber-reinforced concrete under compression. Journal of materials in civil engineering, 4(4), 415-429.

Grime, G. (1934). The measurement of impact stresses in concrete. Proceedings of the Physical Society, 46(2), 196-203.

H. Wu, X. Zhuang, W. Zhang, Z. Zhao. Anisotropic ductile fracture: Experiments, modeling, and numerical simulations, Journal of Materials Research and Technology, 20: 833-856, 2022. https://doi.org/10.1016/j.jmrt.2022.07.128

Hibbitt H D, Karlsson B I, Sorensen E P. ABAQUS user's manual. Providence (RI): Dassault Systemes Simulia Corp., 2013.

Jin, L., Zhang, R., Dou, G., Xu, J., & Du, X. (2018). Experimental and numerical study of reinforced concrete beams with steel fibers subjected to impact loading. International Journal of Damage Mechanics, 27(7), 1058-1083.

Kantar, E., Erdem, R. T., & Anıl, Ö. (2011). Nonlinear finite element analysis of impact behavior of concrete beam. Mathematical and Computational Applications, 16(1), 183-193.

Lee, J., & Fenves, G. L. (1998). Plastic-damage model for cyclic loading of concrete structures. Journal of engineering mechanics, 124(8), 892-900.

Li, H., Chen, W., Pham, T. M., & Hao, H. (2021). Analytical and numerical studies on impact force profile of RC beam under drop weight impact. International Journal of Impact Engineering, 147, 103743.

Lubliner, J., Oliver, J., Oller, S., & Onate, E. (1989). A plastic-damage model for concrete. International Journal of solids and structures, 25(3), 299-326.

M. Badshah, S. Badshah, S. Jan. Comparison of computational fluid dynamics and fluid structure interaction models for the performance prediction of tidal current turbines, Journal of Ocean Engineering and Science 5, 164–172, 2020. https://doi.org/10.1016/j.joes.2019.10.001

Mander, J. B. (1983). Seismic design of bridge piers.

MC2010, F. I. B. (2013). CEB-FIB Model Code for Concrete Structures 2010. Lausanne: International Federation for Structural Concrete.

Meng, K., Xu, L., & Chi, Y. (2021). Experimental investigation on the mechanical behavior of hybrid steel-polypropylene fiber reinforced concrete under conventional triaxial cyclic compression. Construction and Building Materials, 291, 123262.

Najah, A. S. A. (2018). Experimental and analytical investigation on impact behavior of conventional and steel fiber reinforced concrete beams. Atılım University, Institute of Natural Sciences, PhD Thesis.

Naraganti, S. R., Pannem, R. M. R., & Putta, J. (2019). Impact resistance of hybrid fibre reinforced concrete containing sisal fibres. Ain shams engineering journal, 10(2), 297-305.

Saatci, S., & Vecchio, F. J. (2009). Effects of shear mechanisms on impact behavior of reinforced concrete beams. ACI structural Journal.

Saravanakumar, P., Sivakamidevi, M., Meena, K., & Yamini, S. P. (2021). An experimental study on hybrid fiber reinforced concrete beams subjected to torsion. Materials Today: Proceedings, 45, 6818-6821.

Shaaban, I. G., Said, M., Khan, S. U., Eissa, M., & Elrashidy, K. (2021, August). Experimental and theoretical behaviour of reinforced concrete beams containing hybrid fibres. In Structures (Vol. 32, pp. 2143-2160). Elsevier.

Serdar, A. H., Saribiyik, M., Demirtas, G., & Caglar, N. (2021). Çelik Fiber İlaveli Betonarme Kirişlerin Çarpma Yükleri Altındaki Davranışının Doğrusal Olmayan Analizi. Academic Perspective Procedia, 4(2), 214-221.

SETRA-AFGC – Bétons fibrés à ultra-hautes performances. UHPFRC. Recommendations provisoires. Interim Recommendations, January 2002.

Sivakumar, V., Karthik, K., Jachin, S. B., & Xavier, C. A. (2021). WITHDRAWN: Experimental investigation on strength properties of hybrid fibre reinforced high strength concrete.

Tokgoz, S. (2015). Tests on plain and steel fiber concrete-filled stainless steel tubular columns. Journal of Constructional Steel Research, 114, 129-135.

Ulzurrun, G. S., & Zanuy, C. (2017). Enhancement of impact performance of reinforced concrete beams without stirrups by adding steel fibers. Construction and building materials, 145, 166-182.

Vivas, J. C., & Zerbino, R. (2022). Compressive resistance level effect on impact performance of fi-ber reinforced concrete. Revista De La Construcción. Journal of Construction, 21(1), 135–144. https://doi.org/10.7764/RDLC.21.1.135.

Yoo, D. Y., & Banthia, N. (2017). Mechanical and structural behaviors of ultra-high-performance fiber-reinforced concrete subjected to impact and blast. Construction and building materials, 149, 416-431.